RAA 2015 Vol. **15** No. **9**, 1525–1536 doi: 10.1088/1674–4527/15/9/009
http://www.raa-journal.org *http://www.iop.org/journals/raa*

Research in Astronomy and Astrophysics

Case studies of EUV cyclones and their associated magnetic fields

Xin-Ting Yu[1,2], Jun Zhang[1], Ting Li[1] and Shu-Hong Yang[1]

[1] Key Laboratory of Solar Activity, National Astronomical Observatories, Chinese Academy of Sciences, Beijing 100012, China; *liting@nao.cas.cn*
[2] School of Earth and Space Science, University of Science and Technology of China, Hefei 230026, China

Received 2014 September 26; accepted 2015 February 5

Abstract EUV cyclones are rotating structures in the solar corona, and they are usually rooted in the underlying rotating network magnetic fields in the photosphere. However, their connection with the surrounding magnetic fields remains unknown. Here we report an observational study of four typical cyclones which are rooted in different kinds of magnetic fields. We use *Solar Dynamics Observatory*/Atmospheric Imaging Assembly data to investigate the rotation of EUV features in cyclones and Helioseismic and Magnetic Imager data to study the associated magnetic fields. The results show that, (1) an EUV cyclone rooted in a sunspot rotates with the photospheric magnetic field; (2) two EUV cyclones in two faculae of an active region are connected to the same sunspot of the active region but rotate oppositely; (3) an EUV cyclone is rooted in a coronal hole with weak open magnetic fields; (4) a pair of conjugated cyclones is rooted in magnetic fields that have opposite polarity with opposite directions of rotation. The differences in the spatial extent of a cyclone, characteristics of its rotation and underlying fields indicate that cyclones are ubiquitous over the solar atmosphere and that the magnetic structures relevant to the cyclones are more complicated than expected.

Key words: Sun: activity — Sun: corona — Sun: magnetic fields — Sun: photosphere

1 INTRODUCTION

Observations from various space-borne telescopes over the last 20 years have indicated that rotating motions are widely distributed over the Sun. The rotating motions have been discovered in the photosphere as vortices (Brandt et al. 1988; Bonet et al. 2008), in the chromosphere as tiny tornadoes (Wedemeyer-Böhm et al. 2012), in the transition region as swirling transition region jets (spicules) or "explosive events" (Curdt & Tian 2011; Curdt et al. 2012; Dere et al. 1989) and in the corona as twisted jets (Patsourakos et al. 2008; Scullion et al. 2009; Liu et al. 2009; Nisticò et al. 2009; Liu et al. 2011; Shen et al. 2011), surges (Zhang et al. 2000), macrospicules (Pike & Harrison 1997; Pike & Mason 1998; Banerjee et al. 2000; Murawski et al. 2011) and cyclones (Zhang & Liu 2011). They have been seen at different latitudes, both near the equator and near the polar regions (Yu et al. 2014). These rotating activities also have very distinct spatial scales, varying from about $1''$ for vortices in the photosphere to hundreds of arcsec for cyclones and giant tornadoes (Li et al. 2012; Su et al. 2012)

in the corona. Wedemeyer et al. (2013) constructed a power law describing how the abundance is related to the spatial extent of the rotating structures, i.e., the larger the rotating structure, the less widely similar structures like it are distributed.

In the observation and numerical simulation results of Wedemeyer-Böhm et al. (2012), they co-located the chromospheric and coronal swirls in different layers of the Sun. The numerical model of the rotation with different spatial scales from below the photosphere to the lower corona showed that the rotating motions in different layers of the Sun are actually responses to the same effect, the "bathtub effect" (Nordlund 1985). This mechanism can be interpreted as follows. After the plasma cools down and sinks below the solar surface, it forms vortex flows in the intergranular lanes (Stein & Nordlund 1998). This phenomenon is caused by the random walks of the granules surrounding the downward flow, giving the flow a non-zero angular momentum with respect to the center of the downdraft, and due to the conservation of the angular momentum, the plasma starts swirling.

As a specific kind of rotating phenomenon, cyclones in the quiet Sun have been found by Zhang & Liu (2011) in observations from the Atmospheric Imaging Assembly (AIA; Lemen et al. 2012) on board the *Solar Dynamics Observatory* (*SDO*; Pesnell et al. 2012). They also co-located cyclones in the underlying magnetic fields using magnetograms produced by the Helioseismic and Magnetic Imager (HMI; Schou et al. 2012; Scherrer et al. 2012). In fact, the underlying rotating network magnetic fields (RNFs) govern the evolution of the above cyclones. Where there is a cyclone, there must exist an RNF in the photosphere (Zhang & Liu 2011), but the cyclones are more difficult to observe than the RNFs.

Cyclones are often accompanied by brightening during their evolution, which indicate magnetic reconnection and energy release. In some specific cases, waves are detected (Zhang & Liu 2011), and they have also been observed in other swirling phenomena that have different layers (De Pontieu et al. 2007; McIntosh et al. 2011). With energy release and waves that propagate the energy, the rotating motions may provide a mechanism to heat the corona (Wedemeyer-Böhm et al. 2012) and even facilitate the fast solar wind.

From time to time, if one RNF is strong and causes nearby magnetic fields with the same polarity to converge, it may last for a longer time and thus produce a series of cyclones which sequentially appears, e.g., the homologous cyclones described by Yu et al. (2014). This phenomenon exists widely near both the solar equator and the poles. In contrast to cyclones that are triggered by rotating motions in the quiet Sun, rotating motions in active regions (ARs), such as rotating sunspots, have been studied extensively since being first observed by Evershed (1910). The underlying magnetic fields associated with photospheric sunspots have been analyzed based on various observational data and can not only transport energy to the corona (Tian et al. 2008), but also directly drive the process of flares (Yan et al. 2008; Ruan et al. 2014).

In this study we focus on the relationship between several typical cyclones and their underlying and nearby magnetic fields. Using AIA and HMI data, we selected four cases. The first case displays an EUV cyclone in a rotating sunspot. The second case shows two EUV cyclones in two faculae of AR 11801, which are connected to the same sunspot but rotate oppositely. The third case shows a cyclone rooted in a coronal hole, and the last case displays two EUV cyclones with opposite directions of rotation that are rooted in magnetic fields with opposite polarity, named conjugated cyclones. Section 2 describes the observations and results, and the conclusions and discussion are presented in Section 3.

2 OBSERVATIONS AND RESULTS

SDO/AIA presents the full-disk data in 10 wavelengths, providing observations at different temperatures and heights, with a cadence of 12 s and a sampling rate of $0.6''$ pixel^{-1}.

Among these 10 wavelengths, 171 Å images best show the loop structures of EUV cyclones. Therefore we focus on this channel in this study. Moreover, other channels including 193 Å, 211 Å

and 131 Å are also used to analyze the multi-wavelength appearance of EUV cyclones. The underlying RNFs are investigated from the full-disk line-of-sight (LOS) magnetograms of HMI on board *SDO*. These LOS magnetograms have a cadence of 45 seconds and a sampling rate of $0.5''$ pixel^{-1}.

2.1 A Cyclone Rooted in a Sunspot

The first cyclone analyzed here occurred in AR 11973 from 20:00 UT 2014 February 7 to 18:00 UT February 8. It was rooted in a sunspot and the rotating structures of the cyclone could be observed in four EUV channels, 171 Å, 193 Å, 211 Å and 131 Å (Fig. 1(a)–(j)). Two couples of loop structures showed an evident rotation motion around the sunspot (Fig. 1(a)–(c)). The loop structures seemed to connect the negative sunspot with its eastern positive polarity fields. The two loop systems rotate counterclockwise one after another. From 00:10:11 UT to 02:10:11 UT on February 8, the leading loop structure rotates for $25^\circ \pm 3^\circ$ (with angular velocity of $13^\circ \pm 2^\circ$ per hour), while the following loop appeared. During the next time section from 02:10:11 UT to 03:40:11 UT, the first one rotated for $16^\circ \pm 3^\circ$ and the following one for $44^\circ \pm 19^\circ$. The rotation speed can be affected by many factors, such as flux emergence, cancelation, solar rotation, etc. If an RNF rotates slowly and lasts for a long time, the measurement of the rotation speed will be obviously affected by these factors. Viewed in higher-temperature channels, the 211 Å images (see Fig. 1(g)–(i)) only show blurred fronts of the loops. But in 131 Å images (see Fig. 1(d)–(f)), the two corresponding loops are visible but much less evident than in the 171 Å images. This indicates that the 131 Å channel also responds to a lower temperature since the dominant contribution of 131 Å for the AR spectrum comes from continuum emission, with a significant contribution from Fe VIII lines ($T \sim 0.4$ MK).

The underlying sunspot also rotates counterclockwise, in the same direction as the EUV cyclone. In Figure 1(j)–(l), there is a hollow region in the rounded rotating structure. The hollow region rotated from the upper to the east side of the sunspot, whose boundary was tracked to obtain the rotation angle. It was a rotation of $20^\circ \pm 4^\circ$ from 02:08:40 UT to 04:25:10 UT and then a $18^\circ \pm 2^\circ$ rotation to 09:37:10 UT.

To further investigate the rotations of the cyclone and its underlying sunspot, we made two time-slice maps respectively for AIA 171 Å and HMI magnetograms (Fig. 2). In Figure 2(a), the X-axis refers to time, running from 20:00 UT February 7 to 8:00 UT February 8, and the Y-axis refers to the angles measured counterclockwise from 0° to 180°, following the part of the circle shown in Figure 1(a). In Figure 2(a), the white dotted line outlines the first loop system of the cyclone, while the black one outlines the second loop system. The first loop system rotated for 90° from about 21:00 UT on February 7 to 02:00 UT the next day, with an average angular speed of approximately 18° h^{-1}. The second rotating loop structure rotated 60° from about 02:00 UT to 04:30 UT on February 8, with an average angular velocity of around 24° h^{-1}. The two loop systems showed very distinct rotating features, and the first one rotated slower than the second one and showed a gentler acceleration process.

For the slice of the HMI magnetograms in Figure 2(b), the X-axis denotes time running from 23:00 UT February 7 to 17:00 UT February 8, while the Y-axis shows the angles also measured counterclockwise from 30° to 240°. Like what we did for the rotation structure in Figure 1(j)–(l), we tracked the back boundary and found a 90° rotation angle for 18 h and angular velocity of 5° h^{-1}. The magnetic structure maintained an approximately constant velocity through the whole rotational process.

2.2 Two Cyclones Rooted in Two Faculae of an AR

Cyclones rooted in faculae near the AR may interact with the same sunspot, but show very distinct rotating features. Here we first describe this phenomenon that occurred on 2013 July 28. The AR 11801 extends from 12°E to 38°E, and 12°S to 30°N. Both of the two cyclones have a spatial extent

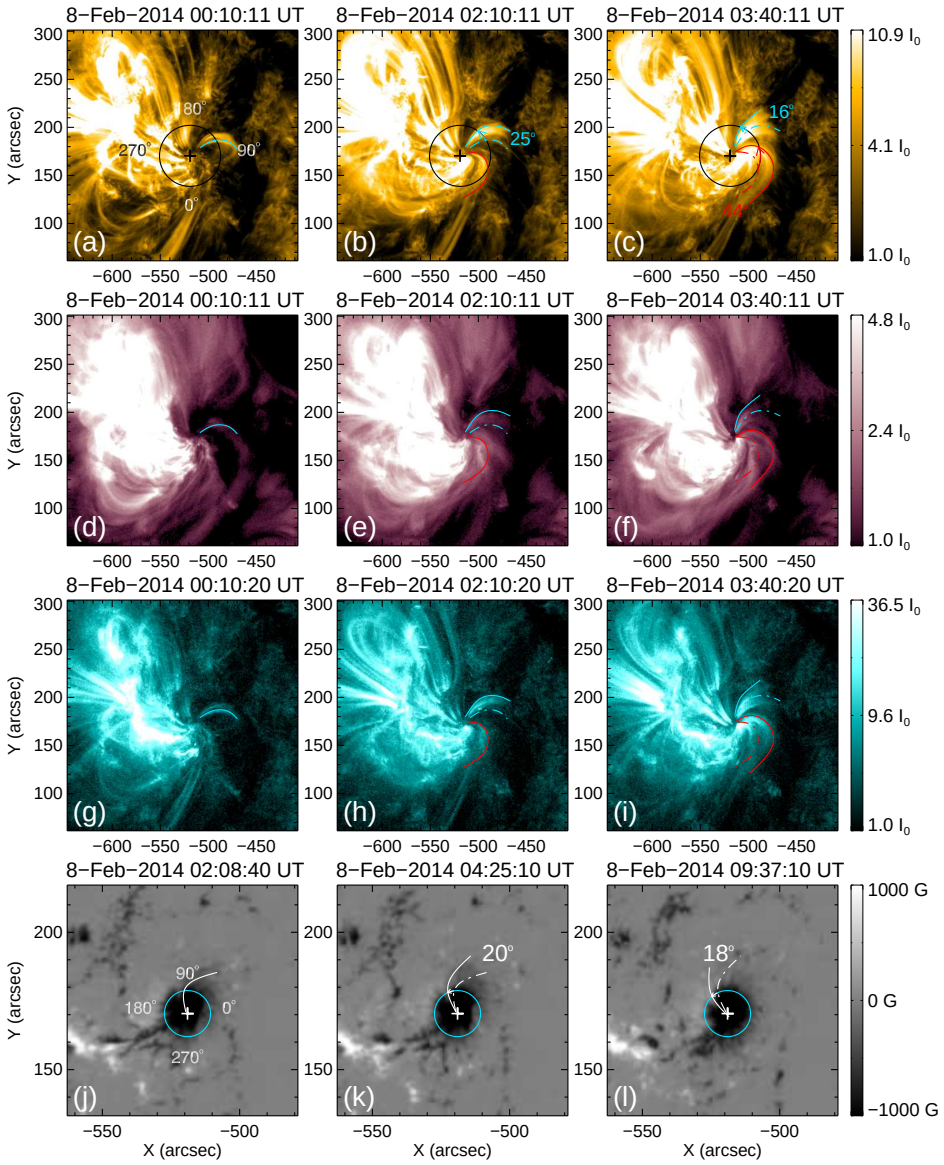

Fig. 1 Panels (a)–(c): AIA 171 Å images (with intensity on a logarithmic scale) showing the cyclone rooted in a rotating sunspot of AR 11973 on 2014 February 8. The blue and red curves represent the two separate structures that are part of the cyclone. The dash dotted curves in panels (b) and (c) are the respective duplicates of the solid curves in panels (a) and (b). The three circles are centered on the magnetic centroid (marked by the black plus) in panels (j)–(l). They also show the position where a time-slice map is made in Fig. 2(a). Panels (d)–(f): corresponding logarithmic AIA 211 Å images. The curves are duplicates of the ones in panels (a)–(c). Panels (g)–(i): corresponding logarithmic AIA 131 Å images. The curves are also duplicates of the ones in panels (a)–(c). Panels (j)–(l): corresponding HMI magnetograms showing the rotation of the underlying magnetic fields at a level of 1000 G. The white pluses represent the position of the magnetic centroid, which is at the center of the three circles. The circles denote the position where the time-slice map is made in Fig. 2(b). The solid and dot dashed curves have similar meanings as those in panels (a)–(c) and they show the evolution of a hollow structure in the magnetograms.

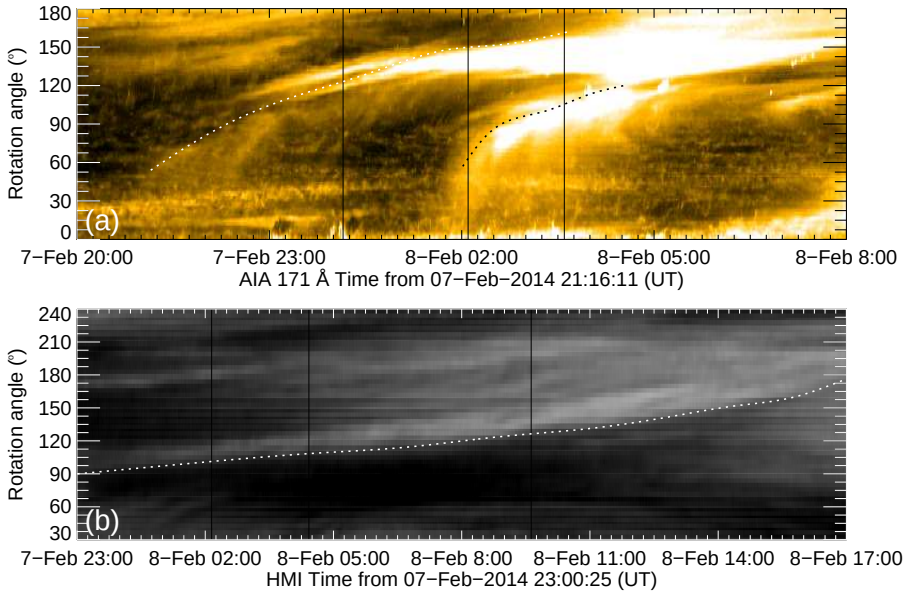

Fig. 2 Panel (a): A time-slice map made from AIA 171 Å images. The X-axis denotes the time running from 20:00 UT 2014 February 7, to 08:00 UT February 8. The Y-axis marks the angle at the center of the circle shown in Fig. 1(a), from 0° to 180° in a counterclockwise direction. The two dashed curves outline two loop systems of the EUV cyclone. The three vertical black lines denote the three chosen times from panels (a)–(c) in Fig. 1. Panel (b): a time-slice map made from HMI magnetogram images. The X-axis denotes the time running from 23:00 UT 2014 February 7, to 17:00 UT February 8. The Y-axis marks the angle measured at the center of the circle shown in Fig. 5(b), from 30° to 240° in a counterclockwise direction. The curve outlines the hollow structure of the sunspot's magnetic fields. The three vertical black lines denote the three chosen times in Fig. 1(j)–(l).

of about 50″. One is north of the AR, and the other is northwest of the AR. From July 27 to July 30, the sunspot of the AR is connected with several cyclones rooted in nearby faculae from time to time. At 18:00:11 UT on July 28, two cyclones (cyclone A and cyclone B) were simultaneously connected to the sunspot as depicted in Figure 3(a). The corresponding magnetograms showed that they are rooted in two faculae with positive polarity, which connect to the strong negative sunspot fields (Fig. 3(b)). The evolution of cyclone A is displayed in Figure 3(c)–(d). Two salient structures are outlined as the green and red curves in Figure 3(c), and the direction of rotation for each structure is also indicated. With the whole patch spinning clockwise from 07:15:11 UT to 10:15:11 UT on July 28, the red curve swirled outward while the green one spun inward. As a result, they moved towards each other as viewed in a 2D plane as shown in Figure 3(d). Its underlying magnetic fields showed a conspicuous rotation of $89°\pm6°$ in 14 h, with an angular velocity of $6°\pm1°$ h^{-1} (Fig. 3(e)–(f)). Cyclone B rotated very fast, $74°\pm5°$ counterclockwise in two hours, with an angular velocity up to $37°\pm3°$ h^{-1} (see Animations 1: *http://www.raa-journal.org/docs/Supp/Animation1.mpg* and 2: *http://www.raa-journal.org/docs/Supp/Animation2.mpg*). The spin of its underlying magnetic fields is $89°\pm5°$ from 11:14:10 UT to 14:14:10 UT with an angular velocity of $30°\pm2°$ h^{-1}, a little slower than the corresponding EUV cyclone.

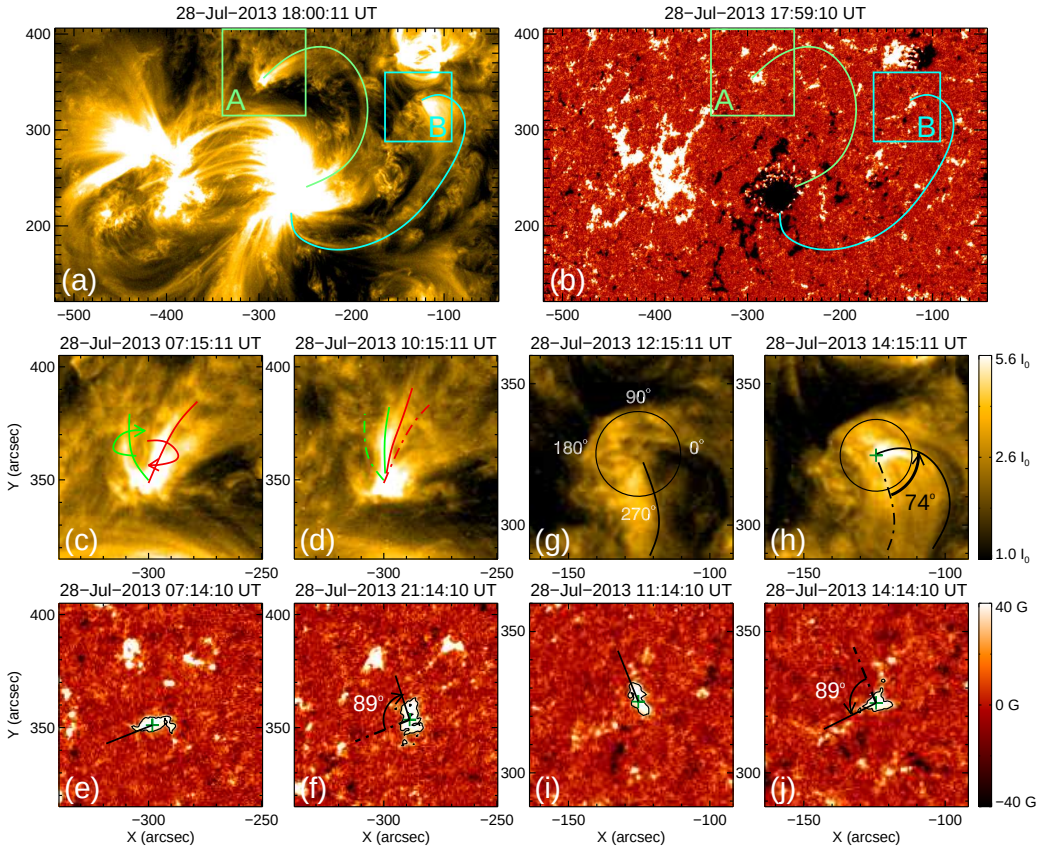

Fig. 3 Panel (a): AIA 171 Å image showing the two cyclones rooted in two faculae and their nearby AR 11801 on 2013 July 28. The two solid curves outline the two loops. The green and blue squares respectively show the FOV of cyclone A in panels (c)–(f) and cyclone B in panels (g)–(j). Panel (b): corresponding HMI magnetogram showing the connectivity between the strong and two weak fields. The curves and two squares are duplicates of those shown in panel (a). Panels (c)–(d): the rotating features of cyclone A (see the accompanying Animation 1). The meanings of different symbols are similar to those in Fig. 1. The directions of rotation for the two boundary structures are indicated by the two arrows in panel (c). Panels (e)–(f): the corresponding underlying magnetic fields. The green pluses mark the magnetic centroid, and the black curves outline the main magnetic field patch at a level of 40 G. The solid lines represent the directions of the longer axis in the contoured area and the dot dashed line is a duplicate of the solid line shown in panel (e). Panels (g)–(j): the rotating features of cyclone B (see the accompanying Animation 2). The meanings of different symbols are similar to those in panels (e)–(f).

2.3 A Cyclone Rooted in Weak Open Fields

As revealed in Figure 4(a), a cyclone is located in a coronal hole region. The coronal hole is in the northern hemisphere of the solar surface, and extends from approximately 48°E to 28°W, and from 4°N to 64°N. A cyclone rooted in open fields of the coronal hole often shows a distinguished shape. Unlike the umbrella-like opening structures of cyclones appearing at the solar equator, it displays needle-like upward structures like the ones in solar polar regions (Yu et al. 2014).

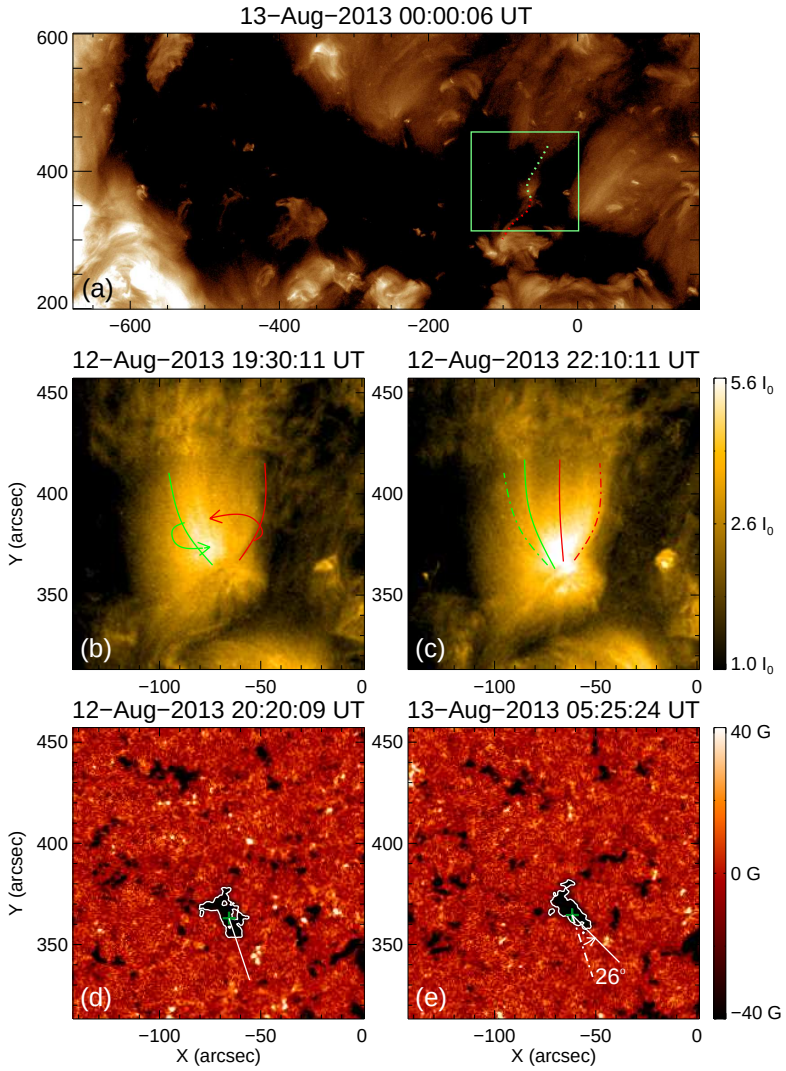

Fig. 4 Panel (a): AIA 193 Å image shows the coronal hole on 2013 August 13. The two dotted curves outline two loop structures which may connect the cyclone's magnetic field with the nearby fields. The green square denotes the field of view (FOV) of panels (b)–(e). Panels (b)–(c): AIA 171 Å images showing the cyclone in the coronal hole. The meanings of the solid and dash dotted curves are similar to those in Fig. 1. Panels (d)–(e): the meanings of different symbols are similar to those in Fig. 3.

As Figure 4(a) displays, the cyclone analyzed here is located in the green box that outlines the coronal hole region and its spatial extent is about 50″. The green and red dotted curves in panel (a) trace two loop structures which may connect the cyclone's magnetic field with the nearby fields, and thus the magnetic field underneath the cyclone is not totally open. However, since the cyclone is located in a coronal hole, the majority of its magnetic field is open. In panels (b)–(c), the rotation of the cyclone is exhibited. It rotated counterclockwise for about half a circle, denoted by

the brightening structure rotating from east to west. Due to the projection effect, we cannot clearly measure the angle that the cyclone rotated, but its underlying magnetic fields show a conspicuous rotation. Here we outline the corresponding magnetic fields and calculate their magnetic centroid. Considering the whole main path to be an oval, we can determine its longer axis. Then we calculate its rotation by measuring the angle between the two rotating longer axes. The spatial extent of the fields is so small and their boundary not only evolves with the rotation of the fields but also with the change of their shape, thus it is more accurate to measure the rotation with the longer axes than the rotation of boundary structures. Here we measured the rotation angle 10 times and took the standard deviation as the uncertainty. A $26^\circ \pm 3^\circ$ rotation is obtained between 20:20:09 UT on August 12 and 05:25:24 UT on August 13, with an angular speed of approximately 3° h^{-1}.

2.4 Two Cyclones Rooted in A Pair of Opposite Fields

Cyclones rooted in RNFs are commonly seen, but in our case, there are two cyclones rooted in RNFs with opposite polarity fields, which are connected by EUV loops. Here we call this pair of cyclones "conjugated cyclones," since they have similar cyclone structures but opposite directions of rotation and polarity. A pair of conjugated cyclones that appeared on 2013 May 12 is displayed in detail in this subsection. In Figure 5(a)–(c), the evolution process of the loops connecting the two rotating conjugated cyclones is shown. The east cyclone rotated counterclockwise and the west cyclone rotated clockwise. Their connecting loop (the blue dotted curves outline the boundary of the loop) raised and twisted. The loop connects the positive magnetic field in the east with the negative magnetic field in the west, and expands during the three subsequent time periods.

We further display the rotating features of each of the conjugated cyclones in Figure 6. The rotation of the east conjugated cyclone is shown in Figure 6(a)–(b). The arm of the cyclone exhibits a spiral structure. From 22:10:11 UT to 23:20:11 UT on May 12, the leading boundary of the spiral structure reveals conspicuous rotation in the counterclockwise direction. The corresponding underlying magnetic field structure rotates $45^\circ \pm 4^\circ$ during a 2 h time interval in Figure 6(d)–(e), with an angular velocity of $23^\circ \pm 2^\circ$ h^{-1}. In the west conjugated cyclone, since there is a bright structure covering the cyclone, only part of its loop appears. Here we exhibit the rotation during a 10-minute time interval. The 171 Å loop structure rotated clockwise, and its underlying magnetic fields showed an approximately $8^\circ \pm 3^\circ$ rotation clockwise during the 10-minute time interval.

3 DISCUSSION AND CONCLUSIONS

Our findings indicate that EUV cyclones are widely distributed in the solar atmosphere and they can be rooted in different kinds of magnetic fields. We have observed cyclones rooted in a rotating sunspot of AR 11973, in open fields of a coronal hole, in a pair of close fields of a quiet region and in faculae of AR 11801. Also, the underlying magnetic fields of some cyclones are connected to the nearby fields, e.g., the pair of rotating fields relevant to the conjugated cyclones is connected to each other by an EUV loop, and the two faculae are connected to the sunspot.

During the past several decades, the swirling or twisting motion in different layers of the solar atmosphere has been widely studied. Rotating phenomena in diverse solar atmospheric layers, like tiny vortices in the photosphere (Bonet et al. 2010), giant vortices in the photosphere (Brandt et al. 1988), magnetic tornadoes in the chromosphere (Wedemeyer-Böhm et al. 2012) and giant tornadoes (Su et al. 2012; Li et al. 2012) probably correspond to the same physical mechanism: sinking plasma swirls due to conservation of angular momentum, and the swirls could have triggered the rotation of the magnetic fields. The rotating magnetic fields then pass the rotation feature from the photosphere upward to the chromosphere, the transition region and even to the solar corona (Wedemeyer-Böhm et al. 2012). These rotating motions have also been counted and statistically follow a power law (Wedemeyer et al. 2013), such that rotating structures with large spatial extents are usually less widely distributed than small rotating structures.

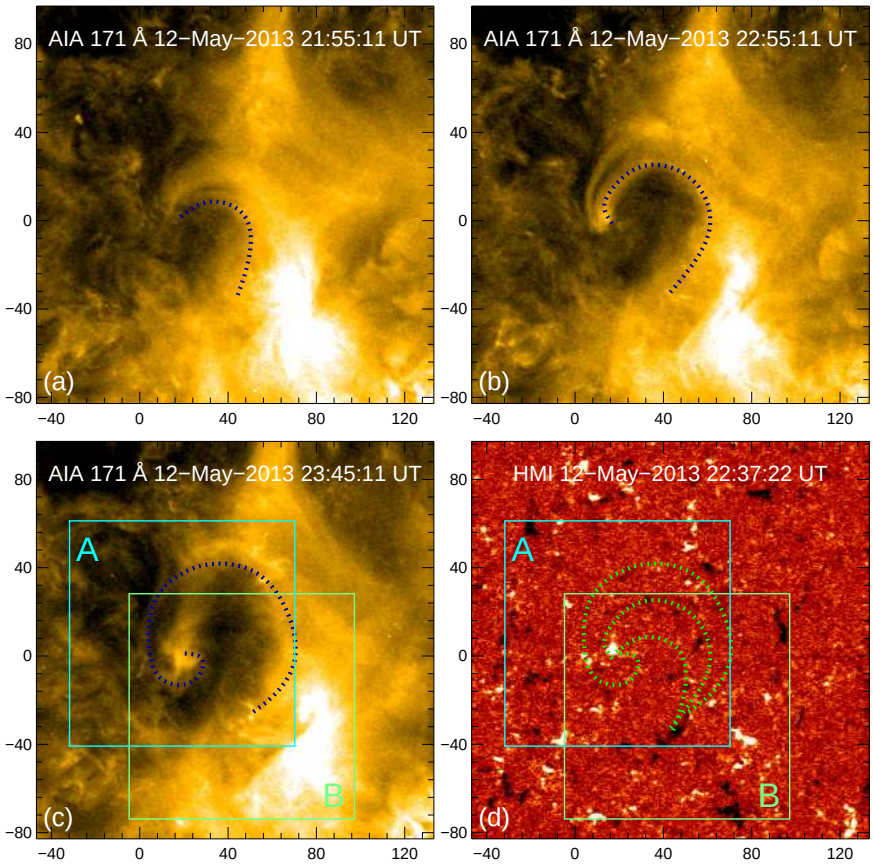

Fig. 5 Panels (a–c): AIA 171 Å image showing the evolution and connectivity of the conjugate cyclones on 2013 May 12. The blue dotted curve in each panel outlines the boundary of the loop between the two cyclones. Panel (d): the corresponding HMI magnetogram. The three green dotted curves are duplicates of the curves in panels (a)–(c).

The rotating features of sunspots are widely obtained by tracing the rotation of the umbrae and preumbrae of sunspots in white light images (Brown et al. 2003; Yan & Qu 2007; Zhang et al. 2007), but are rarely clearly seen in the above EUV wavelengths. But in our work, the sunspot rotation that occurred on 2014 February 8 clearly corresponds to a cyclone in 171 Å, 211 Å and 193 Å. This may be caused by the following reason. Unlike the sigmoid structures that can easily erupt (Canfield & Pevtsov 1999; Brown et al. 2003), this sunspot has a comparatively simple loop structure. It displayed few eruptions which thus made the evolution of the two distinctive rotating boundaries easy to track over a long period of time. Additionally, we found that the rotating angular velocity of the sunspot (5° h^{-1}) is evidently slower than the above rotating cyclones (18° h^{-1} and 24° h^{-1}). Furthermore, the sunspot kept almost a uniform velocity but the cyclones underwent an evident acceleration process. These observational results show that, in the photospheric level, the sunspot rotates approximately as a rigid body (Foukal 1972). At higher solar altitudes where gas pressure is lower, the scale of the rotating features became larger and the rotation became faster.

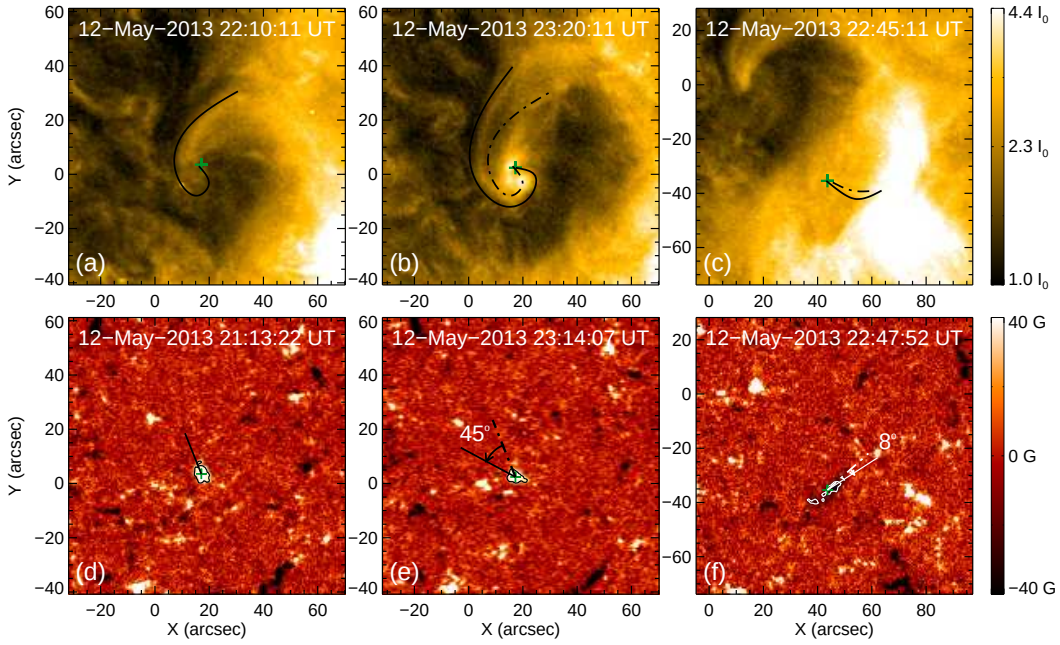

Fig. 6 Panels (a–c): AIA 171 Å images showing the conjugate cyclones on 2013 May 12. Panels (a) and (b) show the evolution of the east cyclone (its FOV is indicated by the blue square in Fig. 5(c)–(d)), while panel (c) shows the west one (its FOV is indicated by the green square in Fig. 5(c)–(d)). The curves and pluses have similar meanings as those in Fig. 1. The dash dotted curve in panel (c) traces the same structure of the west cyclone 10 minutes earlier. Panels (d–f): The corresponding HMI magnetograms. The lines, curves and pluses have similar meanings as those in Fig. 3, except that the dash dotted line in panel (e) represents the direction of the longer axis in the magnetogram 10 minutes earlier.

Compared with the quiet Sun, coronal holes have lower density and temperature (Munro & Withbroe 1972). They show characteristic open magnetic fields, mainly dominated by one polarity. Thus the cyclone we observed in the coronal hole region (see Fig. 4) is different from the cyclones in the quiet Sun, since it displayed needle-like upward structures owing to its distinctive open magnetic fields. Furthermore, if there is energy released from the coronal holes, the energy would be transported through the open field lines, and thus may become the energy source for high-speed solar wind (Krieger et al. 1973). The cyclone we observed in the coronal hole is indeed associated with EUV brightenings, which indicates energy release after reconnection, and this energy could be the source of the fast solar wind.

The occurrence of two RNFs being connected with each other is first reported in this work. We suggest that the two RNFs may be located in two vortices with opposite flows, thus forming two RNFs with opposite directions of rotation. The loop system connecting the two RNFs with opposite polarity became twisted and the two legs of the twisting loop appeared as a pair of conjugated cyclones. With the two cyclones rotating, the connecting loop elevated, elongated and twisted to a certain extent. This kind of cyclone is extremely unstable and easily erupts. The pair of conjugated cyclones only has a lifetime of about 5 h, but other cyclones have an average lifetime of 9 to 10 h (Zhang & Liu 2011; Yu et al. 2014).

The sunspots in case 4 with strong fields are found to be connected with two cyclones rooted in two faculae. Cyclone A is toward the north of the sunspot and cyclone B is toward the northwest of

the sunspot (see Fig. 6), and these two cyclones have opposite directions of rotation, e.g., cyclone A rotated clockwise and cyclone B rotated counterclockwise. Also, cyclone A rotated twice and appeared as a homologous cyclone (Yu et al. 2014). The diversity of the rotating features of the two cyclones may also be due to the different flow fields where they are located. The two diverse local flow fields indicate that the solar atmosphere near the ARs is very dynamic and further research is needed in this kind of facular field. Furthermore, rotating facular fields may twist and braid the magnetic field lines (Schrijver 2007) and thus induce magnetic helicity. In our work, the twist and reconnection process of the rotating facular fields cannot be clearly seen due to the low density and the lack of observations of the coronal magnetic fields. But in the photospheric layer, the twisting motions of penumbral filaments (Su et al. 2010) or flux tubes (Canou & Amari 2010) clearly appeared as torsional structures. Those torsional motions could further lead to reconnection between sheared magnetic loops, as revealed in the numerical simulations, which then trigger flare eruptions (Kusano et al. 2004; Kusano 2005). In addition, brightenings and eruptions are also seen in both of the two cyclones at different levels. The helicity introduced by the connection between cyclones and a sunspot is constantly transported to the corona (Pevtsov 2008), which complicates the magnetic field structure and increases the energy storage in ARs. For future study, we plan to employ vector magnetic field observations to reveal the cyclone structures. These observations may show the actual connections and their time evolution. Moreover, magnetic field extrapolation can also provide information on the coronal magnetic field of cyclones.

Acknowledgements The authors are indebted to the NASA/*SDO* program that provided both the AIA and HMI observations. This work is supported by the National Basic Research Program of China under grant 2011CB811403, the National Natural Science Foundation of China (11221063, 11303050, 11303049 and 11203037), the CAS Project KJCX2-EW-T07, and the Strategic Priority Research Program – The Emergence of Cosmological Structures of the Chinese Academy of Sciences, Grant No. XDB09000000.

References

Banerjee, D., O'Shea, E., & Doyle, J. G. 2000, A&A, 355, 1152
Bonet, J. A., Márquez, I., Sánchez Almeida, J., Cabello, I., & Domingo, V. 2008, ApJ, 687, L131
Bonet, J. A., Márquez, I., Sánchez Almeida, J., et al. 2010, ApJ, 723, L139
Brandt, P. N., Scharmer, G. B., Ferguson, S., Shine, R. A., & Tarbell, T. D. 1988, Nature, 335, 238
Brown, D. S., Nightingale, R. W., Alexander, D., et al. 2003, Sol. Phys., 216, 79
Canfield, R. C., & Pevtsov, A. A. 1999, Washington DC American Geophysical Union Geophysical Monograph Series, 111, 197
Canou, A., & Amari, T. 2010, ApJ, 715, 1566
Curdt, W., & Tian, H. 2011, A&A, 532, L9
Curdt, W., Tian, H., & Kamio, S. 2012, Sol. Phys., 280, 417
De Pontieu, B., McIntosh, S. W., Carlsson, M., et al. 2007, Science, 318, 1574
Dere, K. P., Bartoe, J.-D. F., Brueckner, G. E., & Recely, F. 1989, ApJ, 345, L95
Evershed, J. 1910, MNRAS, 70, 217
Foukal, P. 1972, ApJ, 173, 439
Krieger, A. S., Timothy, A. F., & Roelof, E. C. 1973, Sol. Phys., 29, 505
Kusano, K. 2005, ApJ, 631, 1260
Kusano, K., Maeshiro, T., Yokoyama, T., & Sakurai, T. 2004, ApJ, 610, 537
Lemen, J. R., Title, A. M., Akin, D. J., et al. 2012, Sol. Phys., 275, 17
Li, X., Morgan, H., Leonard, D., & Jeska, L. 2012, ApJ, 752, L22
Liu, C., Deng, N., Liu, R., et al. 2011, ApJ, 735, L18
Liu, W., Berger, T. E., Title, A. M., & Tarbell, T. D. 2009, ApJ, 707, L37

McIntosh, S. W., de Pontieu, B., Carlsson, M., et al. 2011, Nature, 475, 477
Munro, R. H., & Withbroe, G. L. 1972, ApJ, 176, 511
Murawski, K., Srivastava, A. K., & Zaqarashvili, T. V. 2011, A&A, 535, A58
Nisticò, G., Bothmer, V., Patsourakos, S., & Zimbardo, G. 2009, Sol. Phys., 259, 87
Nordlund, A. 1985, Sol. Phys., 100, 209
Patsourakos, S., Pariat, E., Vourlidas, A., Antiochos, S. K., & Wuelser, J. P. 2008, ApJ, 680, L73
Pesnell, W. D., Thompson, B. J., & Chamberlin, P. C. 2012, Sol. Phys., 275, 3
Pevtsov, A. A. 2008, Journal of Astrophysics and Astronomy, 29, 49
Pike, C. D., & Harrison, R. A. 1997, Sol. Phys., 175, 457
Pike, C. D., & Mason, H. E. 1998, Sol. Phys., 182, 333
Ruan, G., Chen, Y., Wang, S., et al. 2014, ApJ, 784, 165
Scherrer, P. H., Schou, J., Bush, R. I., et al. 2012, Sol. Phys., 275, 207
Schou, J., Scherrer, P. H., Bush, R. I., et al. 2012, Sol. Phys., 275, 229
Schrijver, C. J. 2007, ApJ, 662, L119
Scullion, E., Popescu, M. D., Banerjee, D., Doyle, J. G., & Erdélyi, R. 2009, ApJ, 704, 1385
Shen, Y., Liu, Y., Su, J., & Ibrahim, A. 2011, ApJ, 735, L43
Stein, R. F., & Nordlund, Å. 1998, ApJ, 499, 914
Su, J., Liu, Y., Zhang, H., et al. 2010, ApJ, 710, 170
Su, Y., Wang, T., Veronig, A., Temmer, M., & Gan, W. 2012, ApJ, 756, L41
Tian, L., Alexander, D., & Nightingale, R. 2008, ApJ, 684, 747
Wedemeyer-Böhm, S., Scullion, E., Steiner, O., et al. 2012, Nature, 486, 505
Wedemeyer, S., Scullion, E., Rouppe van der Voort, L., Bosnjak, A., & Antolin, P. 2013, ApJ, 774, 123
Yan, X. L., & Qu, Z. Q. 2007, A&A, 468, 1083
Yan, X.-L., Qu, Z.-Q., & Kong, D.-F. 2008, MNRAS, 391, 1887
Yu, X., Zhang, J., Li, T., Zhang, Y., & Yang, S. 2014, ApJ, 782, L15
Zhang, J., Li, L., & Song, Q. 2007, ApJ, 662, L35
Zhang, J., Wang, J., & Liu, Y. 2000, A&A, 361, 759
Zhang, J., & Liu, Y. 2011, ApJ, 741, L7